



Deposited via The University of Leeds.

White Rose Research Online URL for this paper:

<https://eprints.whiterose.ac.uk/id/eprint/165529/>

Version: Accepted Version

Article:

Tostevin, R and Mills, BJW (2020) Reconciling proxy records and models of Earth's oxygenation during the Neoproterozoic and Palaeozoic. *Interface Focus*, 10 (4). 20190137. ISSN: 2042-8901

<https://doi.org/10.1098/rsfs.2019.0137>

© 2020 The Author(s). This is an author produced version of an article published in *Interface Focus*. Uploaded in accordance with the publisher's self-archiving policy.

Reuse

Items deposited in White Rose Research Online are protected by copyright, with all rights reserved unless indicated otherwise. They may be downloaded and/or printed for private study, or other acts as permitted by national copyright laws. The publisher or other rights holders may allow further reproduction and re-use of the full text version. This is indicated by the licence information on the White Rose Research Online record for the item.

Takedown

If you consider content in White Rose Research Online to be in breach of UK law, please notify us by emailing eprints@whiterose.ac.uk including the URL of the record and the reason for the withdrawal request.

1 Reconciling proxy records and models of Earth's oxygenation during 2 the Neoproterozoic and Palaeozoic

3 Rosalie Tostevin¹ and Benjamin J. W. Mills²

4 ¹Department of Geological Sciences, University of Cape Town, Rondebosch, Cape Town,
5 South Africa.

6 ²School of Earth and Environment, University of Leeds, Leeds, LS29JT, UK

7

8 **Abstract**

9 A hypothesised rise in oxygen levels in the Neoproterozoic, dubbed the Neoproterozoic
10 oxygenation event (NOE), has been repeatedly linked to the origin and rise of animal life.
11 However, a new body of work has emerged over the past decade that questions this
12 narrative. We explore available proxy records of atmospheric and marine oxygenation, and
13 considering the unique systematics of each geochemical system, attempt to reconcile the
14 data. We also present new results from a comprehensive COPSE biogeochemical model that
15 combines several recent additions, to create a continuous model record from 850–250 Ma.
16 We conclude that oxygen levels were intermediate across the Ediacaran and early
17 Palaeozoic, and highly dynamic. Stable, modern-like conditions were not reached until the
18 Late Palaeozoic. We therefore propose that the terms Neoproterozoic Oxygenation Window
19 (NOW) and Palaeozoic Oxygenation Event (POE) are more appropriate descriptors of the rise
20 of oxygen in Earth's atmosphere and oceans.

21

22 **1. Introduction**

23 Since the Great Oxidation Event, 2.5 – 2.3 billion years ago (Ga), oxygen has been a
24 persistent feature of Earth’s atmosphere¹, but has remained at low levels throughout the
25 Palaeoproterozoic and Mesoproterozoic eras (2.5 – 1.0 Ga). A hypothesised rise towards
26 modern oxygen levels in the Neoproterozoic (1.0 – 0.54 Ga) was dubbed the
27 “Neoproterozoic Oxygenation Event” (NOE)². Evidence for the NOE included broad increases
28 in the average molybdenum and vanadium concentrations in black shales³; an increase in
29 the isotope fractionation between sulfate and pyrite ($\Delta^{34}\text{S}_{\text{SO}_4\text{-pyr}}$)⁴; and Fe speciation
30 evidence for local deep water oxygenation⁵.

31

32 Geochemical data collected over the last decade has disrupted this narrative. Despite an
33 increase in the breadth and depth of proxy data now available, we appear to be further
34 from a consensus on the timing and dynamics of oxygenation. Some proxies support a
35 single, unidirectional step change in oxygen levels, although estimates of the timing span
36 almost 600 Myrs^{6–15}. Other proxy data support a more dynamic system, with large
37 oscillations in oxygen availability^{16–18}.

38

39 How can we reconcile these different proxy records? One possibility is that some of the
40 geochemical data do not record ancient redox conditions, because they have been
41 overprinted by diagenesis and metamorphism. While some published data may be need to
42 be revisited, other geochemical signals are reproducible in samples from different basins
43 (e.g., Uranium isotopes^{18,19}, or redox sensitive trace elements^{7,17,20,21}). In addition,
44 geochemical redox analysis can be paired with petrography or other geochemical data to
45 screen for potential alteration. Another possibility is that we are misinterpreting primary
46 geochemical signals. Because today’s oceans are largely well-oxygenated, proxy systems are

47 calibrated in isolated basins and lakes, and these environments may not provide a
48 reasonable analogue for a globally anoxic deep ocean. Alternatively, each proxy may be
49 capturing different parts of a complex transition, depending on the proxy systematics,
50 marine residence time, reduction potential, and sampling density. Here, we critically
51 evaluate current proxy evidence for Neoproterozoic–Palaeozoic oxygenation, attempt to
52 reconcile the various records, and compare them to the latest biogeochemical modelling
53 results.

54

55 **2. Evaluation of current geochemical evidence**

56 **2.1 Local Marine Geochemical Proxies**

57 Local marine redox proxies record progressive changes within a single basin^{5,22}, but if those
58 changes are driven by local hydrodynamics or changes in productivity, they may not reflect
59 global changes in oxygen availability. When sufficient local proxy data are collected from
60 multiple basins, the compiled data may record a statistically significant change in the
61 average oxidation state of the ocean. However, these proxy records are necessarily biased
62 towards shelf and slope environments, as Proterozoic sediments from the abyssal plain are
63 rarely preserved. Proxies preserved in carbonates, such as I/Ca and Ce anomalies, are
64 further biased towards warm, shallow shelf environments at low latitudes.

65

66 *Iron speciation:*

67 The ratio of highly reactive to total iron preserved in carbonates and shales is indicative of
68 the redox chemistry in the water column directly above the accumulating sediments²³.

69 Robust calibrations of the proxy in modern sediments allows the differentiation of oxic

70 ($Fe_{HR}/Fe_T < 0.22$) and anoxic water masses ($Fe_{HR}/Fe_T > 0.38$), although ambiguous ratios may

71 be generated under high sedimentation or mixing rates (Fe_{HR}/Fe_T 0.22–0.38). For anoxic
 72 water masses, the proportion of pyrite in the highly reactive iron phase can distinguish
 73 between Fe-bearing (ferruginous) and sulfidic (euxinic) anoxia (Table 1). Therefore, “oxic”
 74 conditions identified by iron speciation could potentially incorporate suboxic and well-
 75 oxygenated conditions. Systematic diagenetic biases could be introduced to the iron
 76 speciation record through transformation of unsulfidised highly reactive iron minerals to
 77 less reactive sheet silicates, producing a false oxic signal.

78
 79 A transition towards oxic Fe speciation signals ~580 Ma, recorded in shales deposited on a
 80 continental slope, was thought to pinpoint permanent oxygenation of the deep ocean⁵.
 81 However, as more data have been collected, an increasingly complex picture of spatial and
 82 temporal heterogeneity has emerged. For example, data from basins of the same age in the
 83 Canadian cordillera show no such oxygenation^{21,24}, and younger basins record anoxic waters
 84 impinging onto the shelf²⁵. A recent statistical analysis of 4,700 Fe speciation measurements
 85 from deep water settings across a range of ages and locations has revealed no significant
 86 long term (i.e., 100 Myr) trend towards more oxic conditions across the Neoproterozoic and
 87 early Palaeozoic (Figure 1 and 2)¹⁴. This study has good spatial and temporal coverage from
 88 ~2.1 Ga to 440 Ma, although Silurian–Devonian data come from just two studies and may be
 89 subject to sampling biases (Figure 2)^{7,26}.

90
 91 **Table 1: Summary of proxy systematics**

	Proxy	Responds to	Redox sensitivity	Archives	Systematic bias?
Local/ Regio	Iron speciation	Integrated regional water column redox conditions	Ferruginous anoxia and euxinia	Shales, carbonate	Variab le

		above accumulating sediments			
	I/Ca ratios	Upper ocean oxygen gradients	Hypoxic (<70 $\mu\text{M O}_2$) to suboxic (between manganous and nitrogenous)	Carbonates	False anoxic
	Ce anomalies	Local–regional water column redox at site of carbonate precipitation	Suboxic (manganous)	Carbonates, phosphorites, iron formation	False anoxic
	$\Sigma\text{Fe}^{3+}/\text{Fe}$	Regional deep water oxygen concentrations	Progressive with increasing $\text{O}_2(\text{aq})$	Basalts	False anoxic
	Marine red beds	Regional deep ocean oxygen concentrations following periods of anoxia	Ferruginous anoxia	Marine red beds	
Global marine	$\delta^{238}\text{U}$	Area of global seafloor bathed in anoxic waters	Anoxia	Carbonates, shales	False anoxic
	$\delta^{98}\text{Mo}$	Area of global seafloor bathed in anoxic waters	Euxinia	Shales	False anoxic
	RSE enrichments	Area of global seafloor bathed in anoxic waters	Euxinia (Mo); ferruginous anoxia (Cr, Re, U, V)	Euxinic shales	False anoxic
	$\delta^{82}\text{Se}$	Local redox conditions and size of global–regional oxidised SeO_x^{2-} reservoir.	Ferruginous anoxia	shales	
	$\delta^{34}\text{S}$	Size of global marine sulfate reservoir and global proportional pyrite burial flux	Euxinia, atmospheric O_2	Carbonates, evaporites	Variable
Atmospheric	$\delta^{53}\text{Cr}$	Atmospheric oxygen	>0.1–1% PAL	Shales, ironstones	
	Wildfire record	Atmospheric oxygen	>70% PAL	Charcoal	

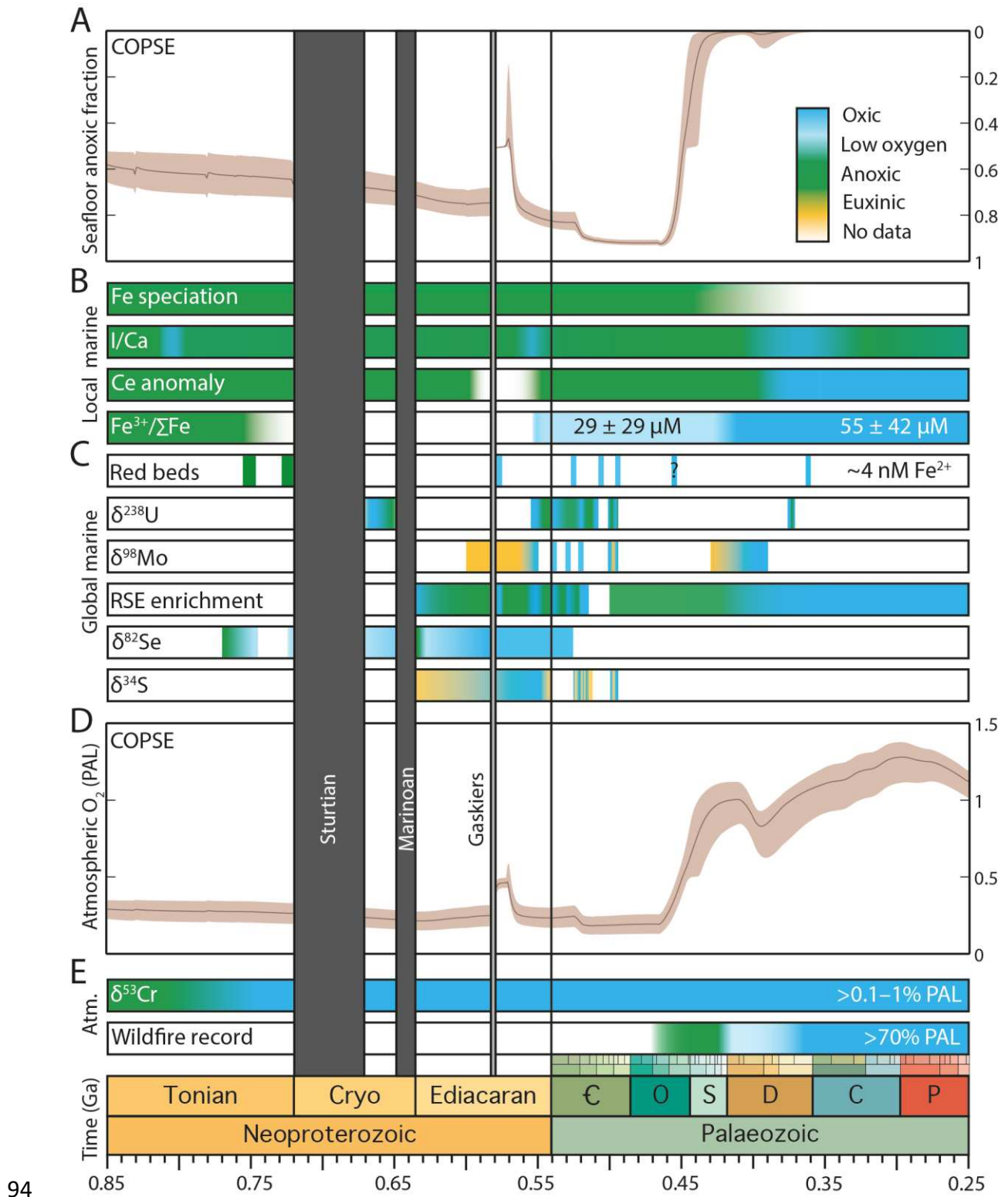
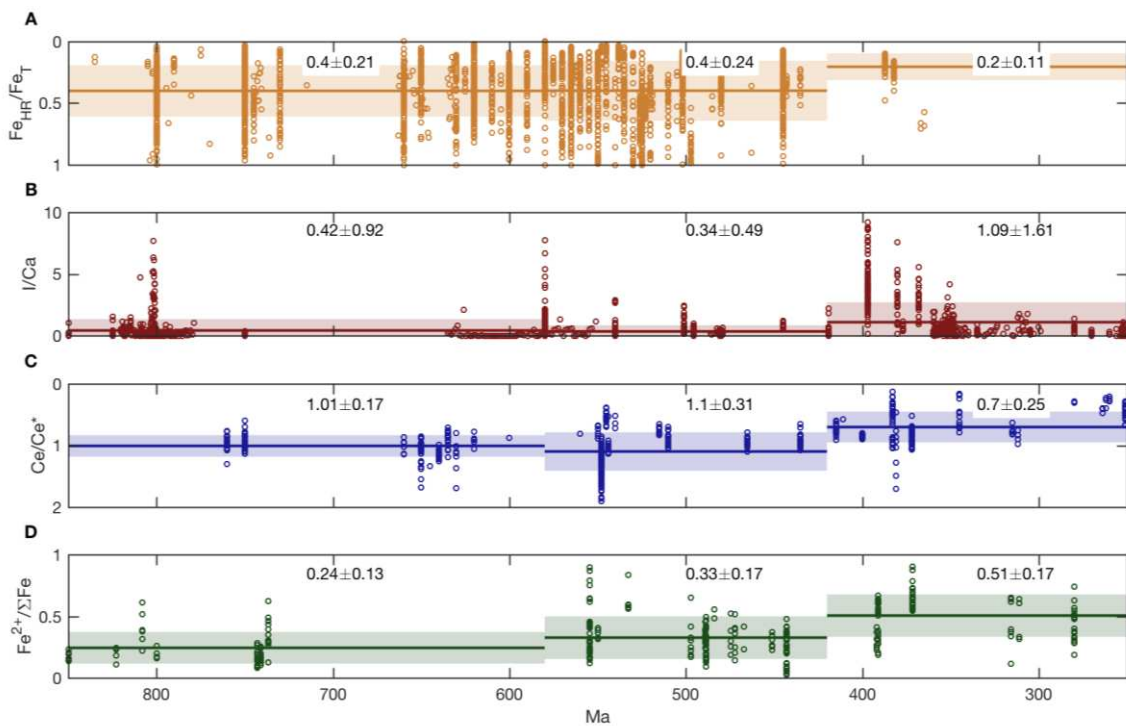


Figure 1. COPSE model predictions of atmospheric and marine redox and inferred redox conditions based on geochemical proxies through the Neoproterozoic and Paleozoic. A.

Modelled sea floor anoxia. Shaded area shows bounds of 10,000 sensitivity analyses. B. Proxy

98 *inferences for local marine oxygenation, indicating dominantly euxinic (yellow), anoxic*
 99 *(green), low oxygen (light blue), and oxic (dark blue) conditions. Surface waters have*
 100 *contained some oxygen since the GOE, but these interpretations represent the dominant*
 101 *redox conditions. Therefore, a green bar does not imply that the entire ocean was anoxic.*
 102 *For interpretation of each data set, and relevant references, see discussion in the text. C.*
 103 *Proxy inferences for global marine oxygenation. D. Modelled atmospheric O₂ (PAL). E. Proxy*
 104 *inferences for atmospheric O₂.*



105
 106 **Figure 2: Geochemical data for local–regional redox proxies from 850–250 Ma.** Data (open
 107 circles) for Fe speciation from shales¹⁴, I/Ca ratios in carbonate rocks^{10,27–29}, Ce anomalies in
 108 carbonate rocks^{30–32} and Fe²⁺/ΣFe ratios of seafloor basalts¹⁵. The average (solid line) and an
 109 error window of 1 standard deviation (shaded region) is shown for time bins 850–580, 580–
 110 420 and 420–250 Ma.

111

112 *I/Ca ratios:*

113 Iodine to calcium ratios in carbonate rocks reflect local water column redox conditions.

114 Since the reduction of iodate (IO_3^-) to iodide (I^-) has a relatively high reduction potential, the

115 *I/Ca* proxy is sensitive to intermediate redox conditions, from hypoxic ($<70\text{--}100\ \mu\text{M O}_2$) to

116 suboxic (manganous – nitrogenous conditions)³³ (Table 1). Iodate is incorporated into

117 carbonate rocks, and so *I/Ca* ratios reflect the oxidised iodate concentration in the local

118 water column at the depth of carbonate formation, which varies with the concentration of

119 oxygen in surface waters and the depth of the top of the OMZ¹⁰. Due to the slow kinetics of

120 iodide oxidation, water masses with fluctuating redox conditions, or anoxia nearby, may

121 retain a low iodate signature, biasing primary signatures towards anoxic conditions. In

122 addition, diagenesis can reduce the *I/Ca* ratio, but not increase it, systematically biasing the

123 rock record towards anoxic conditions²⁷.

124

125 *I/Ca* data span a large range at any given location, but if there are sufficient data, then an

126 increase in the maximum *I/Ca* may indicate oxygenation. Long term compilations reveal

127 variable but low *I/Ca* across the Neoproterozoic and Early Palaeozoic²⁷ (Figure 2), with

128 notable peaks during the Bitter Springs ($\sim 810\text{--}800\ \text{Ma}$)²⁹ and the Shuram excursion (~ 560

129 Ma)^{27,34}. *I/Ca* ratios show a significant peak in the Devonian, between ~ 400 and $\sim 350\ \text{Ma}$,

130 but a return to lower values in the Carboniferous and Permian (Figure 1 and 2)¹⁰. There is no

131 permanent change towards higher *I/Ca* ratios until the early Mesozoic. The maximum *I/Ca*

132 recorded in any given time window may evolve as more data are collected.

133

134 *Ce anomalies*

135 Negative Ce anomalies in rare earth element patterns are indicative of locally oxic water
136 column conditions. Under oxidising conditions, Ce(III) is oxidised to Ce(IV) on the surface of
137 Mn (oxyhydr)oxide minerals, resulting in relative depletion in shale-normalised seawater Ce
138 concentrations compared with the other rare earth elements. The generation of Ce
139 anomalies requires oxidation of Mn and Ce, both of which have relatively high reduction
140 potentials (+1.23 mV and +1.44 mV, respectively). Therefore, Ce anomalies are responsive
141 to the onset of manganoous conditions, which may overlap with low oxygen concentrations
142 (<10 μ M). Ce anomalies can respond to redox changes over meter scales³⁵, although in the
143 open ocean, local signals may be overprinted by basin-wide signals due to slow kinetics³⁰
144 (Table 1). The magnitude of any Ce anomaly may correspond to the concentration of oxygen
145 or the thickness of the oxic layer, but can also be influenced by other factors such as local
146 Mn oxide fluxes³⁶. Rare earth elements, and associated Ce anomalies, substitute for Ca²⁺ in
147 the carbonate mineral lattice, and as such, can faithfully record seawater REE at the site of
148 carbonate formation, and are relatively robust to diagenesis and even dolomitisation^{31,37}.

149

150 A progressive increase in the magnitude of the Ce anomaly after 551 Ma in carbonate rocks
151 from South China was interpreted to record an increase in oxygen levels in the shallow
152 marine environment during the late Ediacaran Period²². However, reducing signals have
153 since been recorded in contemporaneous rocks from the Nama Group, Namibia³²,
154 suggesting oxygenation was not a global phenomenon. Further, long term compilations of
155 Ce anomaly data from eighteen formations show no significant change until the Late
156 Devonian (~383 Ma; Figures 1 and 2)³⁰. However, this broad compilation includes large
157 sample gaps. For example, there is only one sample between ~600 Ma and ~550 Ma.

158

159 *Fe³⁺/ΣFe ratio of submarine basalts*

160 As oxygenated water circulates through seafloor basalts, reduced iron is oxidised to Fe³⁺.

161 Therefore, the Fe³⁺/ΣFe ratio of submarine basalts varies with the magnitude of

162 hydrothermal fluxes and with the oxygen content of bottom waters. As such, seafloor

163 basalts, preserved as ophiolites, can provide a direct record of deep water oxygen

164 concentrations (Table 1). Metamorphism acts to reduce Fe³⁺, and so could systematically

165 bias the Fe³⁺/ΣFe ratio towards lower values.

166

167 Long term compilations of Fe³⁺/ΣFe data show no significant change across the Archean and

168 Proterozoic (Archean = 0.20 ± 0.04; Palaeo–Mesoproterozoic = 0.26 ± 0.02; Neoproterozoic

169 = 0.26 ± 0.05), but a progressive increase across the Early Palaeozoic (0.34 ± 0.08), Late

170 Palaeozoic (0.47 ± 0.10) and Mesozoic–Cenozoic (0.58 ± 0.11) (Figure 2)¹⁵. This indicates a

171 progressive increase in oxygen content of the deep ocean from 11 ± 17 μmolkg⁻¹ in the

172 Neoproterozoic, to 29 ± 29 μmolkg⁻¹ in the Early Palaeozoic, 55 ± 42 μmolkg⁻¹ in the Late

173 Palaeozoic, and 80 ± 53 μmolkg⁻¹ in the Mesozoic–Cenozoic (Figure 1). Due to the

174 distribution of rare ophiolites in the geological record, there are large gaps where no data

175 are available, as well as large uncertainties in the age of some samples. For example, there

176 are no data between 736 ± 1.7 Ma and 554.5 ± 136.5 Ma. In the Stolper and Keller (2018)

177 study, the Neoproterozoic time bin is dominated by samples >700 Ma, but samples between

178 555 and 541 are within range of the Early Palaeozoic average (this is reflected in Figure 1).

179

180 *Red beds:*

181 The distribution of iron rich rocks through the geological record may reflect ocean redox

182 dynamics and Fe²⁺ concentrations¹³. Iron formation requires Fe²⁺ concentrations >50μM,

183 whereas marine red beds, which are thinner and have lower %Fe, only require >4 nM. Major
184 periods of marine red bed deposition occurred in the mid-Ediacaran, Cambrian, and Late
185 Devonian, with a possible event in the late Silurian¹³ (blue on Figure 1). These sporadic
186 events indicate lower deep water Fe concentrations following anoxic events, which could be
187 consistent with more oxygenated deep oceans. This record is biased towards preserved
188 shelf sediments, and may evolve if more examples are documented.

189

190 **2.2 Global Marine Geochemical Proxies**

191 *U isotopes:*

192 The uranium isotope ratio of seawater ($\delta^{238}\text{U}$) is sensitive to the global proportion of
193 seafloor overlain by anoxic bottom waters. During reduction of soluble U(VI) to insoluble
194 U(IV) under anoxic conditions, sedimentary U(IV) is enriched in ^{238}U , leaving seawater
195 depleted in ^{238}U . Therefore, when the anoxic sink expands, seawater $\delta^{238}\text{U}$ decreases, and
196 this signal can be preserved in carbonates. Organic-rich mudrocks also track changes in
197 seawater $\delta^{238}\text{U}$, but the signal is offset by a variable local fractionation factor³⁸ (Table 1).
198 $\delta^{238}\text{U}$ data can be used to calculate the proportion of anoxic seafloor, although these
199 estimates rely on several calibration factors that were determined in modern lakes (e.g., the
200 Black Sea³⁹). In particular, the calculations are sensitive to the isotope fractionation during U
201 reduction, but more work is needed to explore how this varies under euxinic and anoxic
202 ferruginous conditions. Above ~20% seafloor anoxia, the proxy begins to saturate⁴⁰, and
203 large changes in the proportion of seafloor anoxia only translate into small changes in $\delta^{238}\text{U}$.
204 These small changes are within the error introduced by diagenesis⁴¹, which can result in
205 positive $\delta^{238}\text{U}$ offsets of <0.3%.

206

207 Uranium isotope data are available for parts of the Neoproterozoic–Cambrian record (the
208 post-Sturtian interval, and ~560 to ~510 Ma). These data show large oscillations between
209 high, modern-like $\delta^{238}\text{U}$, and very low $\delta^{238}\text{U}$, suggesting that long term anoxia was
210 punctuated by ocean oxygenation events at ~660, ~560, ~540 and ~520 Ma (Figure
211 1)^{9,18,19,40,42,43}. Some of these oscillations are confirmed by multiple studies in different
212 basins^{9,18,19}. Short-term switches towards anoxic conditions are recorded ~497 Ma⁴⁴ and 372
213 Ma⁴⁵. Placing $\delta^{238}\text{U}$ into a quantitative model suggests seafloor anoxia oscillated from >30%
214 during periods of quiescence, to <1% during oxygenation events¹⁸.

215

216 *Mo isotopes:*

217 High $\delta^{98}\text{Mo}$ values preserved in shales indicate globally widespread oxic conditions, under
218 which large negative isotope fractionations occur during adsorption of Mo onto Mn oxides,
219 leaving seawater enriched (Table 1). In contrast, under euxinic conditions, Mo is rapidly and
220 quantitatively removed. Since all known sedimentary Mo sinks have a $\delta^{98}\text{Mo}$ below
221 contemporaneous seawater, $\delta^{98}\text{Mo}$ measurements only provide a minimum constraint on
222 $\delta^{98}\text{Mo}_{\text{sw}}$. Further, interpretations of sedimentary $\delta^{98}\text{Mo}$ rely on independent proxy evidence
223 for local redox conditions. Changes in $\delta^{98}\text{Mo}$ could also result from a switch from euxinic to
224 ferruginous anoxia, with no overall increase in oxygenated waters.

225

226 Pulses in $\delta^{98}\text{Mo}$ are recorded in between ~550 and ~520 Ma, each one reaching
227 progressively higher $\delta^{98}\text{Mo}$ maxima⁶. This was interpreted to indicate progressive marine
228 oxygenation across the Cambrian, but the data contain a lot of scatter, and could also be
229 consistent with discrete oxygenation pulses at ~552, ~540, ~530 and ~521 Ma (Figure 1)^{6,7,9}.
230 Distinguishing between these two scenarios is difficult because the rarity of black shales

231 deposited under fully euxinic conditions limits the resolution of the record. The magnitude
232 of $\delta^{98}\text{Mo}$ enrichments increases through time, suggesting each oxygenation event was more
233 significant than the last⁶. $\delta^{98}\text{Mo}$ reaches stable, modern-like levels between the mid-Silurian
234 and mid-Devonian (~430–390 Ma)⁷. Modelling calculations suggest that oxygenation events
235 in the Neoproterozoic were limited (33% oxic seafloor)^{6,7}, but reached >97% oxic seafloor by
236 ~520 Ma, although many of the parameters in these models are poorly constrained.

237

238 *Redox sensitive elements:*

239 Because Mo is scavenged from seawater under euxinic conditions, and V, U, Re and Cr are
240 scavenged under ferruginous conditions, an increase in the concentration of redox sensitive
241 elements (RSE) in seawater can indicate the global retreat of anoxic sinks. RSE
242 concentrations in shales are controlled by the size of the global RSE reservoir and an
243 enrichment factor, which varies with the local redox conditions. RSE concentrations are
244 commonly analysed in sediments where there is independent evidence for local euxinia, to
245 ensure a consistent local enrichment factor, meaning any enrichments in RSE can be
246 attributed to an expanded global marine RSE reservoir (Table 1). RSE data typically show
247 large amounts of scatter, but an increase in the average or maximum concentration can be
248 interpreted as evidence for an increase in the area of oxic seafloor.

249

250 Long term compilations appeared to show an abrupt increase in Mo, V and U concentrations
251 between 663 and 551 Ma^{3,46}, interpreted to mark widespread oxygenation of the oceans². A
252 recent re-analysis of the U record shows that there is a statistically significant increase in
253 average U concentrations between the Cambrian–Silurian and Devonian–Permian,
254 suggesting any step change towards more permanently oxygenated oceans occurred in the

255 Palaeozoic (Figure 1)^{14,46}. The precise timing of any change will depend on the positions of
256 relatively long timescale bins used for data analysis. However, a more complete
257 stratigraphic record with higher sampling density, from a demonstrably open ocean section
258 in Wuhe, South China, has revealed pulses of RSE enrichment at regular intervals,
259 representing ocean oxygenation events at ~635, ~580, ~560, ~540, ~530 and ~522 Ma
260 (Figure 1)¹⁷. Similar enrichments are observed in other sections located on different cratons,
261 suggesting a truly global signal^{7,20,21}. In between these oxygenation events, the widespread
262 anoxia that characterises much of the Proterozoic returns. Modelling efforts suggest that
263 relatively limited seafloor euxinia (1–10%) and more extensive seafloor anoxia (>30–40%)
264 are needed to crash the global Mo and Cr reservoirs, respectively⁴⁷.

265

266 *Se isotopes:*

267 Se isotopes ($\delta^{82}\text{Se}$) in marine shales are a novel tracer for ocean–atmosphere oxygenation.
268 Se has a reduction potential between S(–II)/S(IV) and Fe(III)/Fe(II), and a relatively short
269 marine residence time (1,100–26,000 years)⁴⁸. During oxyanion (SeO_x^{2-}) reduction under
270 anoxic conditions, isotopically light Se is sequestered into the sediments, driving surface
271 waters isotopically heavy. In addition, an increase in the size of the SeO_x^{2-} reservoir
272 correlates with larger fractionations in locally suboxic sediments (Table 1). Sediments
273 deposited in oxic open oceans, or below well connected OMZs, have lower $\delta^{82}\text{Se}$ than those
274 from restricted anoxic basins, due to the larger SeO_x^{2-} reservoir. $\delta^{82}\text{Se}$ yields insight into the
275 local water column redox conditions, with an additional global control. The signal may be
276 further complicated by variations in riverine input, locally enhanced productivity, or basin
277 restriction.

278

279 A progressive decrease in $\delta^{82}\text{Se}$ is recorded in shales across the Ediacaran, reaching a
280 minimum around the end of the Ediacaran Period¹². For the pre-Gaskiers record, the signal
281 is confirmed in multiple sections, suggesting a global control. This is probably a reflection of
282 an increasing SeO_x^{2-} reservoir, which could reflect ocean oxygenation. Overall, the record is
283 difficult to interpret, but suggests a slow but steady shift from fully anoxic to fully oxic deep
284 waters between ~750 and ~540 Ma.

285

286 *S isotopes:*

287 Under euxinic conditions, microbial sulfate reduction converts sulfate (SO_4^{2-}) into sulfide
288 (HS^-), which may be buried as pyrite. The $\delta^{34}\text{S}$ of seawater sulfate is sensitive to the global
289 pyrite burial flux, and the isotope fractionation associated with that pyrite burial. Both of
290 these parameters are closely tied to ocean–atmosphere redox (Table 1). The $\delta^{34}\text{S}$ signature
291 of seawater is complex⁴⁹, but higher $\delta^{34}\text{S}_{\text{SO}_4}$ could indicate enhanced pyrite burial, which
292 may be driven by expanded euxinia. Large offsets between $\delta^{34}\text{S}_{\text{SO}_4}$ and $\delta^{34}\text{S}_{\text{pyr}}$ ($\Delta^{34}\text{S}_{\text{SO}_4\text{-pyr}}$)
293 have been interpreted to result from a larger marine sulfate reservoir, as well as complex
294 sulfur cycling associated with oxidative side of the S cycle, both of which are associated with
295 higher oxygen levels. At modern marine sulfate concentrations, the $\delta^{34}\text{S}$ of seawater should
296 be globally homogeneous, and is preserved in carbonate rocks and evaporites.

297

298 Sedimentary records shows a progressive increase in $\Delta^{34}\text{S}_{\text{SO}_4\text{-pyr}}$ across the Ediacaran (635–
299 ~550 Ma)⁸, interpreted to represent an increase in the marine sulfate reservoir, and then
300 the onset of oxidative sulfur cycling. The $\Delta^{34}\text{S}_{\text{SO}_4\text{-pyr}}$ decreases again in the late Ediacaran
301 (~550 Ma), along with an increase in $\delta^{34}\text{S}_{\text{SO}_4}$, suggesting increased pyrite burial and a return
302 to anoxia⁵⁰. However, subsequent work has questioned the link between $\Delta^{34}\text{S}_{\text{SO}_4\text{-pyr}}$ and

303 oxidative sulfur cycling⁵¹. A series of rapid oscillations in $\delta^{34}\text{S}_{\text{SO}_4}$ are recorded 524–512 Ma¹⁶,
304 coincident with excursions in with $\delta^{13}\text{C}_{\text{carb}}$, where the rising limbs are associated with
305 periods of ocean anoxia and increased pyrite burial. This increase in net pyrite burial would
306 produce a pulse of atmospheric oxygen, in turn driving anoxia from the shelf. Further $\delta^{34}\text{S}_{\text{SO}_4}$
307 oscillation are recorded ~500 Ma⁴⁴. Sulfur isotopes therefore support dynamic redox
308 conditions into the Cambrian and beyond.

309

310 **2.3 Constraints on atmospheric oxygen**

311 *Cr isotopes*

312 The oxidation and reduction of Cr between Cr(III) and Cr(VI) results in large fractionations.
313 Cr oxidation occurs through dissolution of Cr(III) in soils and reaction with Mn oxides, the
314 presence of which is linked to free O₂. This yields dissolved Cr(VI) species (CrO_4^{2-} and HCrO_4^-
315) that are more soluble, and enriched in the heavy isotope, compared with Cr(III). Therefore,
316 under reducing conditions, the marine Cr record in shales and ironstones will be dominated
317 by unfractionated crustal Cr(III), whereas under an oxidising atmosphere, the Cr record will
318 be isotopically enriched.

319

320 The long term $\delta^{53}\text{Cr}$ record shows a marked enrichment between 800 and 750 Ma¹¹,
321 recorded in both shales and ironstones, and interpreted to indicate a rise in atmospheric O₂
322 concentrations. Although the pre-800 record is dominated by low $\delta^{53}\text{Cr}$, isolated examples
323 of ^{53}Cr enrichments have been recorded⁵². Cr(III) oxidation during weathering is dependent
324 on Mn oxide availability. Quantitative modelling suggests Mn oxide formation occurs at low
325 O₂ (>0.1–1% PAL), providing a maximum constraint on pre-800 Ma atmosphere¹¹, and
326 suggesting a modest increase in atmospheric O₂ around 800–750 Ma.

327

328 *Wildfire record*

329 Wildfires can only be sustained when atmospheric oxygen levels are high (>15–17%)⁵³.

330 Charcoal, the geological expression of palaeo-wildfires, is present in the geological record

331 from the latest Silurian onwards⁵⁴. Charcoal is low in abundance across the Silurian and

332 Devonian, but increases by 1–2 orders of magnitude in the late Devonian⁵⁵. This suggests

333 oxygen crossed a critical threshold in the Late Silurian (>15%), but rose further in the Late

334 Devonian (>17%). Wildfires are dependent on the presence of land plants, which evolved

335 ~470 Ma, so the charcoal record cannot constrain pre-Ordovician pO₂.

336

337

338 **3. Reconciling proxy records**

339 Direct proxies for atmospheric oxygen are scarce. Chromium isotopic fractionations indicate

340 that O₂ rose above 0.1–1% of present atmospheric levels (PAL) at around 800 Ma¹¹,

341 however earlier evidence for fractionation of chromium has been recorded⁵². More certain

342 is a rise in O₂ to >70% PAL during the Late Silurian, and a final rise towards modern levels in

343 the Devonian (>80% PAL or above)^{55,56}. Regardless of atmospheric oxygen concentrations,

344 substantial spatial and temporal variability is expected in marine redox conditions, as water

345 column O₂ is controlled by a balance between the oxygen supply and its utilization during

346 remineralization. Modelling calculations suggest that widespread deep ocean oxygenation

347 requires atmospheric oxygen to exceed 30–40% PAL, but this depends on the availability of

348 the limiting nutrient phosphate⁵⁷, and on the model itself. That said, to first order, deep

349 water oxygenation would be expected to track a substantial rise in atmospheric oxygen

350 levels.

351

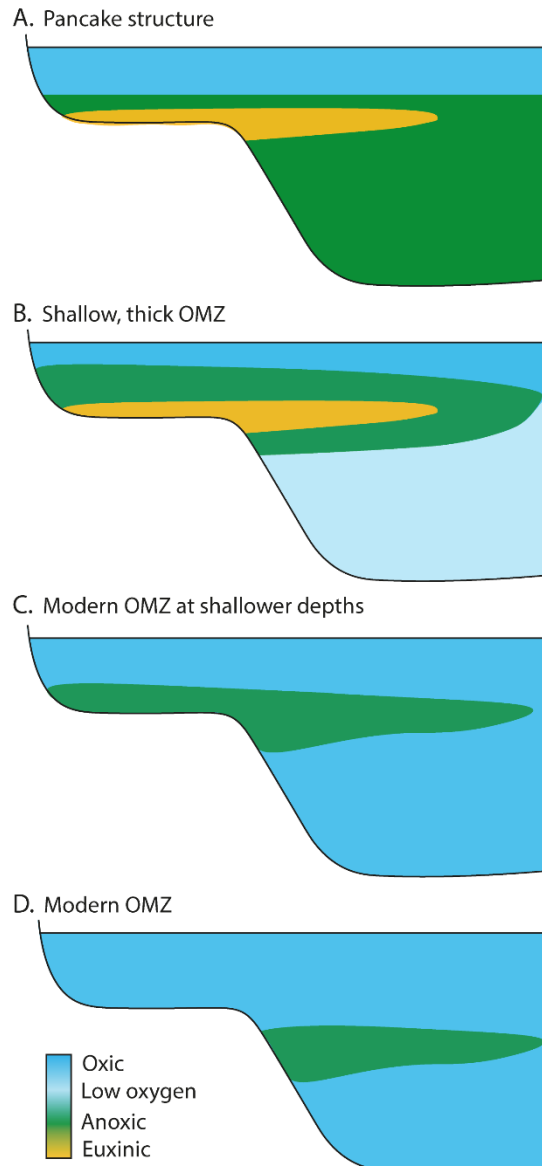
352 Some global marine geochemical proxies record a permanent change towards widespread
353 oxygenation in the late Palaeozoic, including $\delta^{98}\text{Mo}$ and U enrichments^{7,14,46}. Similarly,
354 compilations of local marine redox proxies don't detect any statistically significant change in
355 oxygen availability across the Neoproterozoic, and instead pinpoint widespread marine
356 oxygenation later, in the Late Palaeozoic–Mesozoic: post-Ordovician for Fe speciation¹⁴,
357 Late Devonian for Ce anomalies³⁰, Late Palaeozoic for $\text{Fe}^{3+}/\Sigma\text{Fe}$ ratios¹⁵, and Early Devonian
358 for I/Ca¹⁰. There is some variability in the precise timing recorded by each proxy, which may
359 be accounted for by their different sensitivity to the spatial extent or location of anoxia, or
360 to increasing redox state. More importantly, the timing of oxygenation in long term data
361 compilations is highly sensitive to sampling density as well as the boundaries of data bins.
362 For example, $\text{Fe}^{3+}/\Sigma\text{Fe}$ ratio data are necessarily sparse as they are derived from rare
363 ophiolites. Therefore, these techniques can only be used to make broad comparisons
364 between, e.g., the Early Palaeozoic and Late Palaeozoic. Four compilations of local proxy
365 data, re-analysed using consistent time bins, all show a significant increase in oxygenation in
366 the period 420–250 Ma compared with 580–420 Ma (Figure 2).

367

368 Broadly anoxic Neoproterozoic–Early Palaeozoic oceans could manifest as oxic surface
369 waters overlying fully anoxic deep waters in a 'pancake' structure (Figure 3a), or as shallow,
370 expanded OMZs (Figure 3b and c). A four dimensional transect of local redox conditions
371 across a shelf suggests that OMZ-like structures were established by the Cambrian Period⁵⁸,
372 implying that the deep ocean contained low levels of oxygen. This is consistent with
373 $\text{Fe}^{3+}/\Sigma\text{Fe}$ ratios¹⁵ and the marine red bed record¹³, which support low levels of oxygen in

374 deep waters from the mid-Ediacaran onwards. A shallower OMZ could be a reflection of
375 lower atmospheric oxygen levels, but could also result from differences in carbon cycling.
376

377 If there were indeed mildly oxidising conditions in the deep ocean, then how do we
378 reconcile this with global redox proxies that suggest widespread marine anoxia? Global
379 redox proxies tend to record the percentage of seafloor, globally, that is overlain by anoxic
380 bottom waters, but don't provide insight into the location of those anoxic waters. This is
381 further complicated by the lack of information available on marine productivity, sinking
382 fluxes and ocean circulation, which are key controls on OMZ characteristics. Shallowing of
383 oxygen minimum zones can result in a much larger contact area between anoxic waters and
384 the continental shelf, translating into a larger area of anoxic seafloor, despite no change in
385 the thickness of the OMZ⁵⁹ (Figure 3c and 3d). If the OMZ also expanded in thickness, the
386 combined effect could result in the estimated >10–30% seafloor anoxia and >1% seafloor
387 euxinia required to generate anoxic $\delta^{98}\text{Mo}$, $\delta^{238}\text{U}$ and U-enrichment signals (Figure 3b).
388 Furthermore, if bottom waters in the deep ocean were oxic, but contained only low levels of
389 oxygen (<10 μM), then shallow pore waters would be commonly driven anoxic, which may
390 further contribute to anoxic draw down of RSE such as Mo and U.



391

392

Figure 3. Cartoon showing various possible redox structures for early oceans.

393

394 Although large areas of the seafloor remained anoxic or contained only low levels of oxygen

395 through the Neoproterozoic–Lower Palaeozoic, some proxy systems suggest conditions

396 were dynamic, with brief ocean oxygenation events (OOEs). Some OOEs are recorded

397 independently by multiple proxy systems. For example, the transition back towards anoxic

398 conditions following the ~550 Ma OOE is recorded by $\delta^{98}\text{Mo}$, $\delta^{238}\text{U}$, RSE enrichments, I/Ca

399 ratios and $\delta^{34}\text{S}$ (Figure 1)^{8,9,17,18,27,50}. In contrast, OOEs are not detected in any compilations

400 of local proxy data. For I/Ca ratio and Ce anomaly data, this is likely because sample
401 coverage is too sparse to detect them. For Fe speciation or $\text{Fe}^{3+}/\Sigma\text{Fe}$ ratio data, OOE would
402 not be detected as data are binned into periods orders of magnitude longer than the
403 duration of OOE, so OOE are averaged out or not sampled. Therefore, global redox
404 proxies, analysed in continuous, high resolution sections, detect variability that can be
405 missed by compilations of local redox proxies.

406

407 **4. Modelling the long-term redox transition**

408 Global biogeochemical models can be used to evaluate the processes which have caused
409 the observed oxygenation pattern. The COPSE model⁶⁰ is a non-dimensional system (or 'box
410 model'), which computes the operation of the global C-O-P-S cycles over geological
411 timescales, and is based on the pioneering GEOCARB models^{61,62}. Like GEOCARB, the key
412 considerations for COPSE are the global weathering, burial and degassing processes that
413 control the transfer of key species between the hydrosphere and the crust. The long-term
414 O_2 sources are burial of either organic carbon or pyrite sulfur in sediments (removal of a
415 reductant leads to net oxygenation), and the O_2 sinks are the uplift and weathering, or
416 subduction and degassing, of these reduced species which consumes O_2 . Importantly,
417 COPSE differs from the GEOCARB models in that it is a 'forwards' model, meaning that it
418 computes all processes via an internally-consistent set of biogeochemical rules^{63,64}, rather
419 than seeking to infer them directly from the geological record. This means that COPSE can
420 produce estimates of key geochemical proxies such as carbonate $\delta^{13}\text{C}$, sulfate $\delta^{34}\text{S}$ and
421 strontium $^{87}\text{Sr}/^{86}\text{Sr}$, which are then used to test the 'skill' of the model by comparing to
422 geological data.

423

424 The model is subject to ‘external forcings’: the rate of tectonic CO₂ input, continental
425 uplift and paleogeography, exposed lithological classes, and a variety of switches that
426 represent the evolution of different modes of life which affect global biogeochemistry.
427 Recent reviews are available that describe the latest version of the model^{65,66}. Originally
428 COPSE was built for reconstructing the Phanerozoic Earth system, but in the last decade
429 there have been many extensions to apply the model to the late Precambrian. These
430 extensions have tended to focus on single events such as snowball Earth termination⁶⁷ or
431 the (~580 Ma) Shuram negative carbon isotope excursion⁶⁸. We now bring together the key
432 modifications of the model to produce a complete suite of simulations over the
433 Neoproterozoic and Paleozoic (see supplementary material for full explanation of model
434 parameters and differential equations).

435

436 We begin from the model of Mills et al.⁶⁶, which extended the latest major model
437 release⁶⁵ by updating the rates of CO₂ degassing and tectonic uplift with new estimates, as
438 well as revising the link between global climate and chemical weathering rates, informed by
439 Phanerozoic temperature and CO₂ proxies. We then add a function for the evolution of
440 bioturbation during the early Cambrian⁶⁹; a function that represents input of reduced
441 species from the mantle⁷⁰; a deep ocean reservoir of dissolved organic carbon⁶⁸ and an
442 uplift-weathering event of evaporite sulfate coincident with the Shuram negative carbon
443 isotope anomaly⁶⁸. Each of these additions has been made to the model previously in
444 isolation and the reader is referred to the cited work for more details. To summarize:
445 bioturbating animals are assumed to evolve by 520 Ma and are presumed to increase the
446 re-oxidation of sedimentary organic matter, and drawdown of the nutrient phosphorus;
447 reductant input is assumed to scale with the ridge generation rate and consumes O₂; a deep

448 ocean reservoir of dissolved organic carbon (DOC) is assumed to have built up over the
449 Precambrian and is rapidly oxidised when the deep ocean becomes oxic – driving a sharp
450 negative carbon isotope excursion; and a large sulfate input event occurs at 580 Ma due to
451 the uplift and weathering of Tonian-age evaporite giants. Debate continues about whether
452 an enlarged marine DOC reservoir is required in order to explain Neoproterozoic C isotope
453 dynamics⁷¹, and around the timing of the effects of bioturbation⁷². It is hoped that further
454 analytical and modelling efforts will help to fully resolve these questions. Incorporating
455 these mechanisms into a single consistent model is a part of this process.

456

457 Figure 1 shows the combined COPSE model predictions for atmospheric O₂ and seafloor
458 anoxia over the Neoproterozoic and Paleozoic, and compares them to the proxies discussed
459 earlier. The brown shaded area represents the boundaries of a suite of 10,000 model
460 sensitivity analyses in which the major external forcings (uplift, degassing, lithology) are
461 varied by $\pm 20\%$. There is some agreement with the proxies for atmospheric O₂: COPSE
462 predicts (far) above 0.1% PAL for the entire Neoproterozoic, a rise to >70% PAL by the
463 Silurian, and to 100% PAL in the Devonian. This broad pattern is controlled by the evolution
464 of land plants, which are assumed to increase the weathering delivery of the nutrient
465 phosphate (which drives marine productivity), and also the burial of terrestrially-derived
466 organic carbon⁵⁵. Other key features of the atmospheric O₂ predictions are a spike between
467 580–570 Ma, caused by uplift and weathering of evaporite sulfate which stimulates pyrite
468 burial⁶⁸, and a drop during the Cambrian coincident with the evolution of significant
469 bioturbation, which limits organic carbon preservation⁶⁹. The only area of substantial
470 disagreement with proxies is that COPSE does not produce lower atmospheric O₂ before
471 ~800 Ma, whereas the lack of fractionation in the Chromium isotope record suggests O₂

472 might be below 1% PAL¹¹. It is not currently clear how strong the constraint from the Cr
473 isotope record is, given that fractionations have been found in several pre-800 Ma
474 samples⁵², but it is also possible that a major process is still missing from COPSE, which if
475 included, would result in lower atmospheric O₂. There are several candidates here, including
476 the lack of explicit productivity-remineralization dynamics in the ocean, or a better
477 representation of Precambrian tectonics. Research is ongoing.

478

479 The seafloor anoxia prediction from COPSE follows the transitions in atmospheric O₂,
480 with more than 50% of the seafloor anoxic during the Neoproterozoic, and full ventilation
481 during the Devonian. In general agreement with the proxies, there is a period of expanded
482 oxic seafloor immediately post-Gaskiers, which then returns to almost entirely anoxic by the
483 later Cambrian. But there are three major discrepancies between the model predictions and
484 the proxies for seafloor anoxia. Firstly, the model does not produce any of the rapid
485 variability attested to by the proxies (OOEs). Secondly, the model fails to reproduce longer
486 term oxygenation surrounding the Sturtian and Marinoan glaciations. Finally, the model
487 predicts very large anoxic seafloor areas during the later Cambrian and Ordovician, which
488 are not directly supported by any proxies.

489

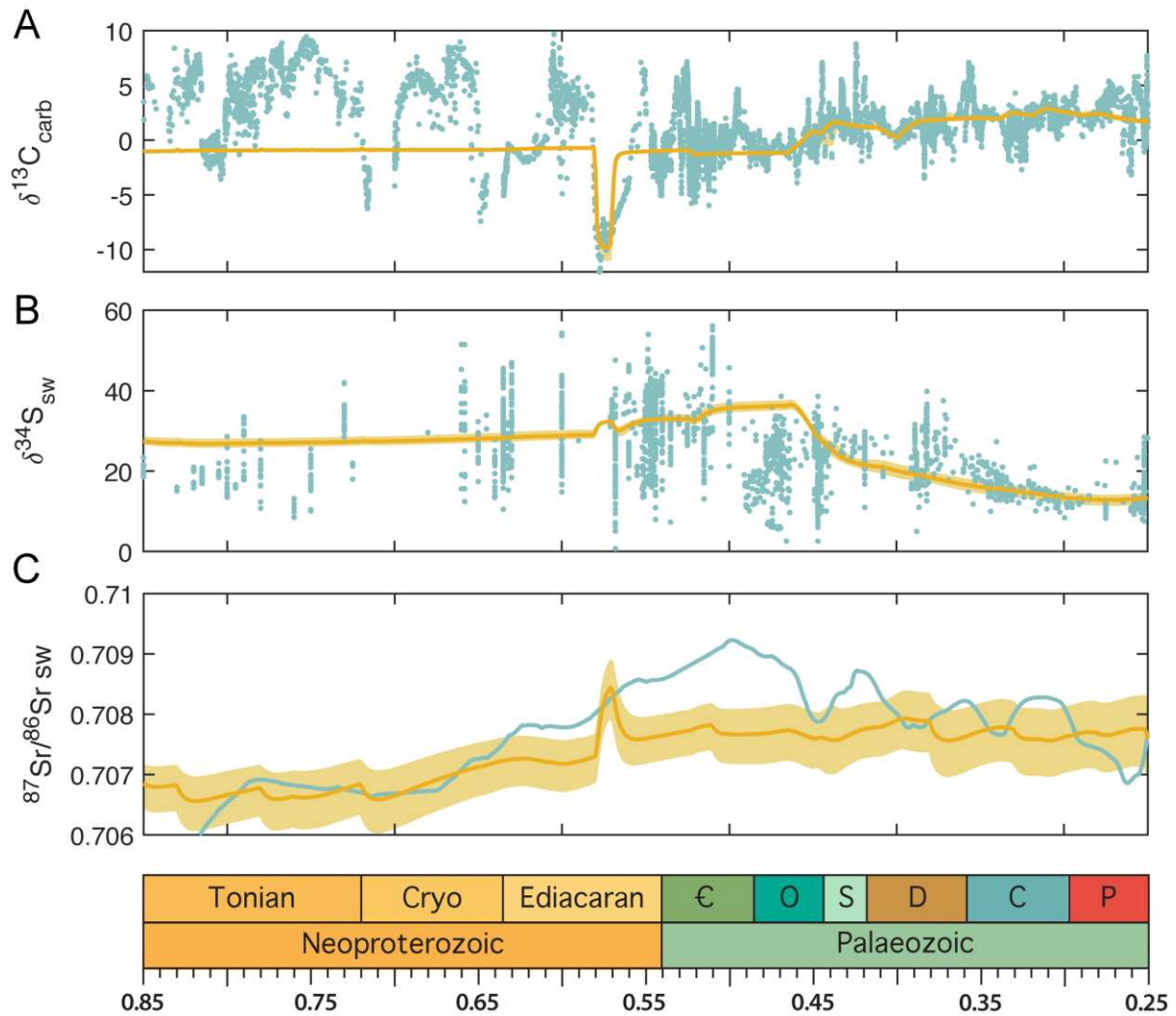
490 The inability of the COPSE model to reproduce the OOEs in the later Ediacaran and
491 Cambrian is probably due to the model's use of a single-box ocean. In COPSE, the shelf
492 environments and (much more vast) deeper ocean are considered to be a single system.
493 This adds a huge amount of buffering capacity, which may not be realistic. A more
494 sophisticated biogeochemical model^{73,74} splits the ocean into multiple boxes representing
495 areas of the shelf, open ocean and deep ocean. This model shows that OOEs can occur due

496 to feedbacks between the marginal phosphorus and oxygen cycles, and thus the lack of
497 OOE in COPSE may be a consequence of limited representation of shelf environments.

498

499 The lack of any appreciable oxygen changes around the Sturtian and Marinoan
500 glaciations is also relatively easily explained, as this version of the COPSE model still does
501 not incorporate any of the processes associated with either the initiation or termination of
502 these snowball Earth events. Looking to the model outputs for sedimentary isotope ratios
503 (Figure 4), it is clear that while the Post-Gaskiers predictions are within reason, the model is
504 missing major aspects of Earth system function pre-600 Ma, especially in the carbon cycle.
505 Here, the large and sustained positive carbon isotope excursions that occur before the
506 Sturtian, and during the aftermath of both glaciations, may represent increased productivity
507 and oxygen production, which is supported by the O₂ proxies.

508



509

510 **Figure 4. COPSE model isotopic outputs.** *Geochemical constraints are shown in teal, and*

511 *model outputs in yellow. A. $\delta^{13}\text{C}$ carbonate sediments. B. $\delta^{34}\text{S}$ seawater sulfate. C. $^{87}\text{Sr}/^{86}\text{Sr}$*

512 *carbonate sediments.*

513

514 An argument could be made that the break-up of the Rodinia supercontinent was

515 underway by $\sim 750 \text{ Ma}$ ⁷⁵ and led to enhanced continental weathering⁷⁶, high rates of organic

516 carbon burial, and high $\delta^{13}\text{C}$, before driving the system towards the Sturtian snowball Earth.

517 It is then possible that CO_2 rose to extremely high levels during the glaciations, meaning that

518 the super-greenhouse period that followed glaciation lasted several 10s of Myrs before CO_2

519 could be reduced to background levels⁶⁷. Adding these ideas into the COPSE model is

520 possible, but in order to reproduce the timing of isotope excursions, the weathering
521 response to temperature and the effect of erosion on weathering must be very carefully
522 chosen. Thus, we defer further investigation of the dynamics and timing of global glaciations
523 and weathering events in the Cryogenian to spatial models with a better approximation of
524 continental weathering (e.g., GEOCLIM^{77,78}).

525

526 The large areas of anoxic seafloor during the Cambrian–Ordovician coincide with
527 carbonate $\delta^{13}\text{C}$ predictions that sit generally below the data, indicating that the model may
528 be underestimating oxygen production (or incorrectly simulating organic C weathering⁷⁹).
529 This may be due to an over-estimate of the importance of bioturbation in re-oxidising
530 sedimentary organic carbon and burying phosphate. New reaction-transport models of the
531 bioturbation process will hopefully help test this.

532

533 **5. Assessing the role of oxygen in early animal evolution**

534 The hypothesised rise in oxygen levels across the Neoproterozoic–Palaeozoic has been
535 repeatedly linked to the origin and radiation of early animals^{5–7,11,16,80}. Given that oxygen is
536 required by all extant animals, this hypothesis seems intuitive and has proved rather
537 attractive. But a large body of recent work has shown that the role of oxygen in early animal
538 ecosystems is more complex than previously thought^{18,81,82}. One issue is that not all
539 geochemical data provide the information needed to address ecologically relevant
540 questions, such as the precise oxygen levels. Waters containing 100 μM or 1 μM O_2 would
541 be indistinguishable in many proxy systems, but the first could host a complex ecosystem
542 containing skeletal animals and motile predators, and the second would be largely
543 uninhabitable^{83,84}. These issues can be partly resolved by considering the systematics of

544 each geochemical proxy, and exactly what information they provide about the redox
545 structure of ancient environments.
546
547 Minimum oxygen levels are necessary, but not sufficient, to explain the appearance of new
548 species or ecological traits. Simple sponge-grade animals have very low oxygen demands (1–
549 10 μM)⁸¹, and these requirements appear to have been met continuously in surface waters
550 from at least 800 Ma onwards¹¹. During the Neoproterozoic, there may have been
551 progressive increase in the maximum dissolved O_2 ; enabling the development of more
552 aerobically demanding traits, such as motility and bioturbation. However, for most of the
553 Ediacaran, many proxies suggest widespread anoxic deep waters^{18,19}. Ecosystem dynamics,
554 animal distributions, and migration patterns will be influenced by this reduction in habitable
555 space, but clearly, early animal communities continued to thrive in shallow, well-oxygenated
556 shelf environments where their oxygen demands were met^{25,32}. It is therefore important to
557 constrain the maximum $\text{O}_2(aq)$ available in shelf environments, as well as the spatial extent
558 of inhospitable environments.

559

560 The marine redox landscape in the Cryogenian and Ediacaran appears to have been highly
561 dynamic. It has been suggested that OOE's could have stimulated evolution, and their
562 frequency appears to increase in the late Ediacaran and Cambrian, coincident with an
563 intense period of diversification¹⁷. Periods of anoxia in between OOE's could even stimulate
564 the development of genetic diversity⁸². Geochemical data and model results suggest that
565 although the Neoproterozoic redox landscape was dynamic, there was no permanent
566 change towards stable, well-oxygenated oceans until at least the Devonian, likely assisted
567 by the evolution of land plants^{7,10,14,15,30,55}.

568

569 **6. Conclusions and future directions**

570 The proxy data are best reconciled in the following way: Atmospheric O₂ reached a
571 concentration of >0.1% PAL by around ~800 Ma, and potentially earlier. Surface waters in
572 contact with this atmosphere contained low levels of dissolved oxygen, but the deep oceans
573 remained anoxic. Atmospheric oxygen probably rose in steps or pulses throughout the
574 Cryogenian and Ediacaran, associated with major events such as the break-up of Rodinia,
575 and the Sturtian, Marinoan and Gaskiers glaciations. The post-Sturtian is also marked by the
576 first brief OOE, which continue into the Cambrian. There is some evidence for OOE
577 magnitude increasing over time⁶, and a gradual rise in oxygen over the Neoproterozoic is
578 also consistent with selenium isotope data¹². By the start of the Cambrian, pO₂ surpassed
579 30–40% PAL, but oxygen concentrations in much of the deep ocean remained low and the
580 OMZ was thick and shallow. Atmospheric oxygen rose again in the Late Silurian, surpassing
581 70% PAL, and rose to modern-like levels in the Devonian, pushing the OMZ back off the shelf
582 and establishing modern, well-oxygenated oceans (Figure 3d). The COPSE model is unable to
583 reproduce the full complexity revealed by geochemical data, but does capture first order
584 patterns of atmospheric and marine oxygenation from the Ediacaran onwards, giving
585 confidence that the behaviour we see in the proxies is reasonable. The hypothesised
586 Neoproterozoic Oxygenation Event (NOE) would be more accurately described as a
587 Neoproterozoic Oxygenation Window (NOW), featuring dynamic pulses of oxygenation
588 against a background of gradually rising oxygen levels, and any step change towards stable,
589 well-oxygenated conditions appears to have been delayed until the Palaeozoic Oxygenation
590 Event (POE).

591

592 Moving forward, we need to consider which geochemical data can best capture this
593 transition. To understand the timing, frequency and duration of OOE's, we need to target
594 high resolution continuous successions and analyse multiple global redox proxies. To
595 meaningfully address questions surrounding the role of oxygen in early animal ecosystems,
596 we need to focus on developing quantitative constraints on maximum $O_2(aq)$. These could
597 include proxies for atmospheric oxygen, such as Cr isotopes, or marine redox proxies that
598 respond to intermediate redox conditions, such as Ce anomalies and I/Ca. Detailed 4D maps
599 across shelf ecosystems can reveal the structure of marine anoxia (i.e., pancake vs. OMZ),
600 and be tied directly to the fossil record.

601

602 **Data accessibility**

603 The geochemical data are all published elsewhere, and discussed in full in the relevant
604 references. Differential equations and fixed parameters from the model are available in the
605 supplementary material. All modelling code and outputs can be obtained from BJWM on
606 request.

607

608 **Author's contributions**

609 R.T. compiled proxy data, and B.J.W.M. modified the COPSE biogeochemical model. R.T. and
610 B.J.W.M discussed the results and wrote the manuscript together.

611

612 **Competing interests**

613 The authors declare no competing interests

614

615 **Acknowledgements**

616 We are grateful to Zunli Lu and Noah Planavsky for reviews that helped to improve this
617 manuscript. We thank the Royal Society for supporting us to attend a meeting in London
618 where these ideas were discussed. R.T. is supported by a grant from the DSI-NRF Centre of
619 Excellence in Palaeosciences and B.J.W.M is funded by the UK Natural Environment
620 Research Council (NE/R010129/1 and NE/S009663/1) and by a University of Leeds Academic
621 Fellowship.

622

623 **References**

- 624 1. Farquhar, J., Bao, H. & Thiemens, M. Atmospheric Influence of Earth's Earliest Sulfur
625 Cycle. *Science* **289**, 756–758 (2000).
- 626 2. Och, L. M. & Shields-Zhou, G. A. The Neoproterozoic oxygenation event: environmental
627 perturbations and biogeochemical cycling. *Earth-Sci. Rev.* **110**, 26–57 (2012).
- 628 3. Scott, C. *et al.* Tracing the stepwise oxygenation of the Proterozoic ocean. *Nature* **452**,
629 456–459 (2008).
- 630 4. Canfield, D. E. & Farquhar, J. Animal evolution, bioturbation, and the sulfate
631 concentration of the oceans. *Proc. Natl. Acad. Sci. U. S. A.* **106**, 8123–8127 (2009).
- 632 5. Canfield, D. E., Poulton, S. W. & Narbonne, G. M. Late-Neoproterozoic Deep-Ocean
633 Oxygenation and the Rise of Animal Life. *Science* **315**, 92–95 (2007).
- 634 6. Chen, X. *et al.* Rise to modern levels of ocean oxygenation coincided with the Cambrian
635 radiation of animals. *Nat. Commun.* **6**, (2015).
- 636 7. Dahl, T. W. *et al.* Devonian rise in atmospheric oxygen correlated to the radiations of
637 terrestrial plants and large predatory fish. *Proc. Natl. Acad. Sci.* **107**, 17911–17915
638 (2010).

- 639 8. Fike, D. A., Grotzinger, J. P., Pratt, L. M. & Summons, R. E. Oxidation of the Ediacaran
640 Ocean. *Nature* **444**, 744–747 (2006).
- 641 9. Kendall, B. *et al.* Uranium and molybdenum isotope evidence for an episode of
642 widespread ocean oxygenation during the late Ediacaran Period. *Geochim. Cosmochim.*
643 *Acta* **156**, 173–193 (2015).
- 644 10. Lu, W. *et al.* Late inception of a resiliently oxygenated upper ocean. *Science* **361**, 174–
645 177 (2018).
- 646 11. Planavsky, N. J. *et al.* Low Mid-Proterozoic atmospheric oxygen levels and the delayed
647 rise of animals. *Science* **346**, 635–638 (2014).
- 648 12. Pogge von Strandmann, P. A. E. *et al.* Selenium isotope evidence for progressive
649 oxidation of the Neoproterozoic biosphere. *Nat. Commun.* **6**, 10157 (2015).
- 650 13. Song, H. *et al.* The onset of widespread marine red beds and the evolution of
651 ferruginous oceans. *Nat. Commun.* **8**, 1–7 (2017).
- 652 14. Sperling, E. A. *et al.* Statistical analysis of iron geochemical data suggests limited late
653 Proterozoic oxygenation. *Nature* **523**, 451–454 (2015).
- 654 15. Stolper, D. A. & Keller, C. B. A record of deep-ocean dissolved O₂ from the oxidation
655 state of iron in submarine basalts. *Nature* **553**, 323 (2018).
- 656 16. He, T. *et al.* Possible links between extreme oxygen perturbations and the Cambrian
657 radiation of animals. *Nat. Geosci.* **12**, 468–474 (2019).
- 658 17. Sahoo, S. K. *et al.* Oceanic oxygenation events in the anoxic Ediacaran ocean. *Geobiology*
659 **14**, 457–468 (2016).
- 660 18. Tostevin, R. *et al.* Uranium isotope evidence for an expansion of anoxia in terminal
661 Ediacaran oceans. *Earth Planet. Sci. Lett.* **506**, 104–112 (2019).

- 662 19. Zhang, F. *et al.* Extensive marine anoxia during the terminal Ediacaran Period. *Sci. Adv.*
663 **4**, eaan8983 (2018).
- 664 20. Kurzweil, F. *et al.* Coupled sulfur, iron and molybdenum isotope data from black shales
665 of the Teplá-Barrandian unit argue against deep ocean oxygenation during the
666 Ediacaran. *Geochim. Cosmochim. Acta* **171**, 121–142 (2015).
- 667 21. Johnston, D. T. *et al.* Searching for an oxygenation event in the fossiliferous Ediacaran of
668 northwestern Canada. *Chem. Geol.* **362**, 273–286 (2013).
- 669 22. Ling, H.-F. *et al.* Cerium anomaly variations in Ediacaran–earliest Cambrian carbonates
670 from the Yangtze Gorges area, South China: implications for oxygenation of coeval
671 shallow seawater. *Precambrian Res.* **225**, 110–127 (2013).
- 672 23. Poulton, S. W. & Canfield, D. E. Development of a sequential extraction procedure for
673 iron: implications for iron partitioning in continentally derived particulates. *Chem. Geol.*
674 **214**, 209–221 (2005).
- 675 24. Canfield, D. E. *et al.* Ferruginous Conditions Dominated Later Neoproterozoic Deep-
676 Water Chemistry. *Science* **321**, 949–952 (2008).
- 677 25. Wood, R. A. *et al.* Dynamic redox conditions control late Ediacaran ecosystems in the
678 Nama Group, Namibia. *Precambrian Res.* **261**, 252–271 (2015).
- 679 26. Boyer, D. L., Owens, J. D., Lyons, T. W. & Droser, M. L. Joining forces: Combined
680 biological and geochemical proxies reveal a complex but refined high-resolution palaeo-
681 oxygen history in Devonian epeiric seas. *Palaeogeogr. Palaeoclimatol. Palaeoecol.* **306**,
682 134–146 (2011).
- 683 27. Hardisty, D. S. *et al.* Perspectives on Proterozoic surface ocean redox from iodine
684 contents in ancient and recent carbonate. *Earth Planet. Sci. Lett.* **463**, 159–170 (2017).

- 685 28. Uahengo, C.-I., Shi, X., Jiang, G. & Vatuva, A. Transient shallow-ocean oxidation
686 associated with the late Ediacaran Nama skeletal fauna: Evidence from iodine contents
687 of the Lower Nama Group, southern Namibia. *Precambrian Res.* 105732 (2020)
688 doi:10.1016/j.precamres.2020.105732.
- 689 29. Lu, W. *et al.* Iodine proxy evidence for increased ocean oxygenation during the Bitter
690 Springs Anomaly. *Geochem. Perspect. Lett.* **5**, 53–57 (2017).
- 691 30. Wallace, M. W. *et al.* Oxygenation history of the Neoproterozoic to early Phanerozoic
692 and the rise of land plants. *Earth Planet. Sci. Lett.* **466**, 12–19 (2017).
- 693 31. Nothdurft, L. D., Webb, G. E. & Kamber, B. S. Rare earth element geochemistry of Late
694 Devonian reefal carbonates, Canning Basin, Western Australia: confirmation of a
695 seawater REE proxy in ancient limestones. *Geochim. Cosmochim. Acta* **68**, 263–283
696 (2004).
- 697 32. Tostevin, R. *et al.* Low-oxygen waters limited habitable space for early animals. *Nat.*
698 *Commun.* **7**, (2016).
- 699 33. Lu, W. *et al.* Refining the planktic foraminiferal I/Ca proxy: Results from the Southeast
700 Atlantic Ocean. *Geochim. Cosmochim. Acta* (2019) doi:10.1016/j.gca.2019.10.025.
- 701 34. Macdonald, F. A. *et al.* The stratigraphic relationship between the Shuram carbon
702 isotope excursion, the oxygenation of Neoproterozoic oceans, and the first appearance
703 of the Ediacara biota and bilaterian trace fossils in northwestern Canada. *Chem. Geol.*
704 **362**, 250–272 (2013).
- 705 35. De Carlo, E. H. & Green, W. J. Rare earth elements in the water column of Lake Vanda,
706 McMurdo Dry Valleys, Antarctica. *Geochim. Cosmochim. Acta* **66**, 1323–1333 (2002).

- 707 36. O'Connell, B., Wallace, M. W., Hood, A. v. S., Lechte, M. A. & Planavsky, N. J. Iron-rich
708 carbonate tidal deposits, Angepena Formation, South Australia: A redox-stratified
709 Cryogenian basin. *Precambrian Res.* **342**, 105668 (2020).
- 710 37. Banner, J. L., Hanson, G. N. & Meyers, W. J. Rare Earth Element and Nd Isotopic
711 Variations in Regionally Extensive Dolomites From the Burlington-Keokuk Formation
712 (Mississippian): Implications for Ree Mobility During Carbonate Diagenesis. *J. Sediment.*
713 *Res.* **58**, (1988).
- 714 38. Lau, K. V., Romaniello, S. J. & Zhang, F. The Uranium Isotope Paleoredox Proxy. *Elements*
715 *in Geochemical Tracers in Earth System Science /core/elements/uranium-isotope-*
716 *paleoredox-proxy/200458FA5D3F890D690C8907FEF738D7* (2019)
717 doi:10.1017/9781108584142.
- 718 39. Rolison, J. M., Stirling, C. H., Middag, R. & Rijkenberg, M. J. A. Uranium stable isotope
719 fractionation in the Black Sea: Modern calibration of the $^{238}\text{U}/^{235}\text{U}$ paleo-redox proxy.
720 *Geochim. Cosmochim. Acta* **203**, 69–88 (2017).
- 721 40. Lau, K. V., Macdonald, F. A., Maher, K. & Payne, J. L. Uranium isotope evidence for
722 temporary ocean oxygenation in the aftermath of the Sturtian Snowball Earth. *Earth*
723 *Planet. Sci. Lett.* **458**, 282–292 (2017).
- 724 41. Chen, X. *et al.* Diagenetic effects on uranium isotope fractionation in carbonate
725 sediments from the Bahamas. *Geochim. Cosmochim. Acta* **237**, 294–311 (2018).
- 726 42. Dahl, T. W. Reorganisation of Earth's biogeochemical cycles briefly oxygenated the
727 oceans 520 Myr ago. *Geochem. Perspect. Lett.* **3**, 210–220 (2017).
- 728 43. Wei, G.-Y. *et al.* Marine redox fluctuation as a potential trigger for the Cambrian
729 explosion. *Geology* **46**, 587–590 (2018).

- 730 44. Dahl, T. W. *et al.* Uranium isotopes distinguish two geochemically distinct stages during
731 the later Cambrian SPICE event. *Earth Planet. Sci. Lett.* **401**, 313–326 (2014).
- 732 45. White, D. A., Elrick, M., Romaniello, S. & Zhang, F. Global seawater redox trends during
733 the Late Devonian mass extinction detected using U isotopes of marine limestones.
734 *Earth Planet. Sci. Lett.* **503**, 68–77 (2018).
- 735 46. Partin, C. A. *et al.* Large-scale fluctuations in Precambrian atmospheric and oceanic
736 oxygen levels from the record of U in shales. *Earth Planet. Sci. Lett.* **369–370**, 284–293
737 (2013).
- 738 47. Reinhard, C. T. *et al.* Proterozoic ocean redox and biogeochemical stasis. *Proc. Natl.*
739 *Acad. Sci.* **110**, 5357–5362 (2013).
- 740 48. Fernández-Martínez, A. & Charlet, L. Selenium environmental cycling and bioavailability:
741 a structural chemist point of view. *Rev. Environ. Sci. Biotechnol.* **8**, 81–110 (2009).
- 742 49. Fike, D. A., Bradley, A. S. & Rose, C. V. Rethinking the Ancient Sulfur Cycle. *Annu. Rev.*
743 *Earth Planet. Sci.* **43**, 593–622 (2015).
- 744 50. Ries, J. B., Fike, D. A., Pratt, L. M., Lyons, T. W. & Grotzinger, J. P. Superheavy pyrite
745 ($\delta^{34}\text{S}_{\text{pyr}} > \delta^{34}\text{S}_{\text{CAS}}$) in the terminal Proterozoic Nama Group, southern Namibia: A
746 consequence of low seawater sulfate at the dawn of animal life. *Geology* **37**, 743–746
747 (2009).
- 748 51. Sim, M. S., Bosak, T. & Ono, S. Large Sulfur Isotope Fractionation Does Not Require
749 Disproportionation. *Science* **333**, 74–77 (2011).
- 750 52. Canfield, D. E. *et al.* Highly fractionated chromium isotopes in Mesoproterozoic-aged
751 shales and atmospheric oxygen. *Nat. Commun.* **9**, 1–11 (2018).
- 752 53. Belcher, C. M. & McElwain, J. C. Limits for Combustion in Low O₂ Redefine
753 Paleatmospheric Predictions for the Mesozoic. *Science* **321**, 1197–1200 (2008).

- 754 54. Glasspool, I. J., Edwards, D. & Axe, L. Charcoal in the Silurian as evidence for the earliest
755 wildfire. *Geology* **32**, 381–383 (2004).
- 756 55. Lenton, T. M. *et al.* Earliest land plants created modern levels of atmospheric oxygen.
757 *Proc. Natl. Acad. Sci.* **113**, 9704–9709 (2016).
- 758 56. Glasspool, I. J. & Scott, A. C. Phanerozoic concentrations of atmospheric oxygen
759 reconstructed from sedimentary charcoal. *Nat. Geosci.* **3**, 627–630 (2010).
- 760 57. Canfield, D. E. A new model for Proterozoic ocean chemistry. *Nature* **396**, 450–453
761 (1998).
- 762 58. Guilbaud, R. *et al.* Oxygen minimum zones in the early Cambrian ocean. *Geochem.*
763 *Perspect. Lett.* **6**, 33–38 (2018).
- 764 59. Lau, K. V. *et al.* Marine anoxia and delayed Earth system recovery after the end-Permian
765 extinction. *Proc. Natl. Acad. Sci.* **113**, 2360–2365 (2016).
- 766 60. Bergman, N. M., Lenton, T. M. & Watson, A. J. COPSE: a new model of biogeochemical
767 cycling over Phanerozoic time. *Am. J. Sci.* **304**, 397–437 (2004).
- 768 61. Berner, R. A. (Yale U. GEOCARB II: A revised model of atmospheric CO₂ over phanerozoic
769 time. *Am. J. Sci. U. S.* **294:1**, (1994).
- 770 62. Berner, R. A. (Yale U. A model for atmospheric CO₂ over phanerozoic time. *Am. J. Sci. U.*
771 *S.* **291:4**, (1991).
- 772 63. Cappellen, P. V. & Ingall, E. D. Benthic phosphorus regeneration, net primary
773 production, and ocean anoxia: A model of the coupled marine biogeochemical cycles of
774 carbon and phosphorus. *Paleoceanography* **9**, 677–692 (1994).
- 775 64. Lenton, T. M. & Watson, A. J. Redfield revisited: 2. What regulates the oxygen content of
776 the atmosphere? *Glob. Biogeochem. Cycles* **14**, 249–268 (2000).

- 777 65. Lenton, T. M., Daines, S. J. & Mills, B. J. W. COPSE reloaded: An improved model of
778 biogeochemical cycling over Phanerozoic time. *Earth-Sci. Rev.* **178**, 1–28 (2018).
- 779 66. Mills, B. J. W. *et al.* Modelling the long-term carbon cycle, atmospheric CO₂, and Earth
780 surface temperature from late Neoproterozoic to present day. *Gondwana Res.* **67**, 172–
781 186 (2019).
- 782 67. Mills, B., Watson, A. J., Goldblatt, C., Boyle, R. & Lenton, T. M. Timing of Neoproterozoic
783 glaciations linked to transport-limited global weathering. *Nat. Geosci.* **4**, 861–864
784 (2011).
- 785 68. Shields, G. A. *et al.* Unique Neoproterozoic carbon isotope excursions sustained by
786 coupled evaporite dissolution and pyrite burial. *Nat. Geosci.* **12**, 823–827 (2019).
- 787 69. van de Velde, S., Mills, B. J. W., Meysman, F. J. R., Lenton, T. M. & Poulton, S. W. Early
788 Palaeozoic ocean anoxia and global warming driven by the evolution of shallow
789 burrowing. *Nat. Commun.* **9**, 1–10 (2018).
- 790 70. Williams, J. J., Mills, B. J. W. & Lenton, T. M. A tectonically driven Ediacaran oxygenation
791 event. *Nat. Commun.* **10**, 1–10 (2019).
- 792 71. Husson, J. M. *et al.* Large isotopic variability at the micron-scale in ‘Shuram’ excursion
793 carbonates from South Australia. *Earth Planet. Sci. Lett.* **538**, 116211 (2020).
- 794 72. Tarhan, L. G. The early Paleozoic development of bioturbation—Evolutionary and
795 geobiological consequences. *Earth-Sci. Rev.* **178**, 177–207 (2018).
- 796 73. Alcott, L. J., Mills, B. J. W. & Poulton, S. W. Stepwise Earth oxygenation is an inherent
797 property of global biogeochemical cycling. *Science* (2019).
- 798 74. Slomp, C. P. & Van Cappellen, P. The global marine phosphorus cycle: sensitivity to
799 oceanic circulation. *Biogeosciences Discuss.* **3**, 1587–1629 (2006).

- 800 75. Li, Z. X. *et al.* Assembly, configuration, and break-up history of Rodinia: A synthesis.
801 *Precambrian Res.* **160**, 179–210 (2008).
- 802 76. Donnadieu, Y., Godd ris, Y., Ramstein, G., N d lec, A. & Meert, J. A ‘snowball Earth’
803 climate triggered by continental break-up through changes in runoff. *Nature* **428**, 303–
804 306 (2004).
- 805 77. Godd ris, Y. *et al.* Onset and ending of the late Palaeozoic ice age triggered by
806 tectonically paced rock weathering. *Nat. Geosci.* **10**, 382–386 (2017).
- 807 78. Godd ris, Y., Donnadieu, Y., Le Hir, G., Lefebvre, V. & Nardin, E. The role of
808 palaeogeography in the Phanerozoic history of atmospheric CO₂ and climate. *Earth-Sci.*
809 *Rev.* **128**, 122–138 (2014).
- 810 79. Daines, S. J., Mills, B. J. W. & Lenton, T. M. Atmospheric oxygen regulation at low
811 Proterozoic levels by incomplete oxidative weathering of sedimentary organic carbon.
812 *Nat. Commun.* **8**, 1–11 (2017).
- 813 80. Nursall, J. Oxygen as a prerequisite to the origin of the Metazoa. *Nature* **183**, 1170–1172
814 (1959).
- 815 81. Mills, D. B. *et al.* Oxygen requirements of the earliest animals. *Proc. Natl. Acad. Sci.* **111**,
816 4168–4172 (2014).
- 817 82. Wood, R. & Erwin, D. H. Innovation not recovery: dynamic redox promotes metazoan
818 radiations. *Biol. Rev.* (2017) doi:10.1111/brv.12375.
- 819 83. Levin, L. A., Gage, J. D., Martin, C. & Lamont, P. A. Macrobenthic community structure
820 within and beneath the oxygen minimum zone, NW Arabian Sea. *Deep Sea Res.* **47**, 189–
821 226 (2000).
- 822 84. Sperling, E. A. *et al.* Oxygen, ecology, and the Cambrian radiation of animals. *Proc. Natl.*
823 *Acad. Sci.* **110**, 13446–13451 (2013).

